ACS Combinatorial Science

Research Article

Cite This: ACS Comb. Sci. XXXX, XXX, XXX−XXX

pubs.acs.org/acscombsci

Fluorescence Multiplexing with Spectral Imaging and Combinatorics

Hadassa Y. Holzapfel,[†,‡] Alan D. Stern,[†] Mehdi Bouhaddou,[†] Caitlin M. Anglin,[§] Danielle Putur,[†] Sarah Comer,[†] and Marc R. Birtwistle*[,†,§]

[†]Department of Pharmacological Sciences, Icahn School of Medicine at Mount Sinai, New York, New York 10029, United States

[‡]Medical School for International Health, Faculty of Health Sciences, Ben-Gurion University of the Negev, Be'er Sheva, 84105, Israel

[§]Department of Chemical and Biomolecular Engineering, Clemson University, Clemson, South Carolina 29634, United States

Supporting Information

ABSTRACT: Ultraviolet-to-infrared fluorescence is a versatile and accessible assay modality but is notoriously hard to multiplex due to overlap of wide emission spectra. We present an approach for fluorescence called **m**ultiplexing **u**sing **s**pectral **i**maging and **c**ombinatorics (MuSIC). MuSIC consists of creating new independent probes from covalently linked combinations of individual fluorophores, leveraging the wide palette of currently available probes with the mathematical power of combinatorics. Probe levels in a mixture can be inferred from spectral emission scanning data. Theory and simulations suggest MuSIC can increase fluorescence multiplexing ∼4−5 fold using currently available dyes and measurement tools. Experimental proof-of-principle demonstrates robust demultiplexing of nine solution-based probes using ∼25% of the available excitation wavelength window (380−480 nm), consistent with theory. The increasing prevalence of white lasers, angle filter-based wavelength scanning, and large, sensitive multianode photomultiplier tubes make acquisition of such MuSIC-compatible data sets increasingly attainable.

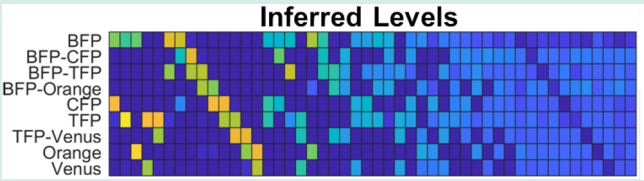

KEYWORDS: *fluorescence multiplexing, spectral imaging, combinatorics*

INTRODUCTION

Fluorescence in the UV to infrared range is one of the most widely used and easily accessible quantitative and qualitative assay modalities across the life and physical sciences.[1] Yet, fluorescence is notoriously hard to multiplex, that is, to measure multiple analytes simultaneously in a mixture. Typical fluorescence multiplexing is routinely limited to about four colors, each corresponding to a single measurement.[2] For example, one of the arguably most multiplexed and data dense experimental modalities—Illumina "next-generation" deep DNA sequencing—relies on such four-color imaging, one for each DNA base.[3] This four-color standard is the case when fluorescence emission is collected via broad-banded filters, as opposed to the entire emission spectra.

When so-called hyper-spectral or fluorescence emission scanning is employed along with linear unmixing,[4,5] measurement of up to seven analytes or even eight is possible.[6−11] Cycles of staining tumor sections with fluorophore-labeled antibodies, coupled with chemical inactivation and multiple rounds of staining, has been reported to analyze 61 antigens.[12] A similar principle has been applied without the use of a proprietary instrument to produce cyclic immunofluorescence that uses repeated rounds of four color imaging for ∼25 analytes.[13]

Specific assay instantiations that separate analytes in a variety of ways have also been able to reach higher multiplexing capabilities. For example, super-resolution imaging combined with *in situ* hybridization and combinatorial labeling used fluorescence to measure 32 nucleic acids in single yeast cells.[14] The Luminex xMAP system can multiplex ∼40 analytes separated by specific beads.[15] Segregating fluorophores by individual bacterium can multiplex ∼28 different strains using "CLASI-FISH."[16] Alternatives to fluorescence are also of course many, for example, mass cytometry, which measures levels of ∼30 specific isotope tags as opposed to fluorophores.[17,18]

Despite these advances, there remains yet to be reported, to our knowledge, a fluorescence-based technology that simultaneously can demultiplex more than four to seven analytes within a mixture. Such an ability may have widespread impact, due to the prevalence, sensitivity, and versatility of fluorescence as a measurement tool. Here, we report such an advance, which we term **m**ultiplexing **u**sing **s**pectral **i**maging and **c**ombinatorics (MuSIC). MuSIC works by creating covalent combinations of existing fluorophores and measuring fluorescence emission spectra of their mixtures. We first describe the theoretical basis for MuSIC, and then through simulation studies explore potential limits of the approach. Finally, we experimentally demonstrate the feasibility of MuSIC to measure the levels of nine different fluorescent probes in a mixture using only ∼25% of the available spectral window of fluorescence excitation (380−480 nm), supporting a potential 5-fold increase in fluorescence multiplexing ability. The advent and accessibility of white lasers, angle filter-based emission wavelength scanning, and large, sensitive multianode photomultiplier tubes make

Received: July 16, 2018
Revised: October 7, 2018
Published: October 19, 2018

DOI: 10.1021/acscombsci.8b00101
ACS Comb. Sci. XXXX, XXX, XXX−XXX

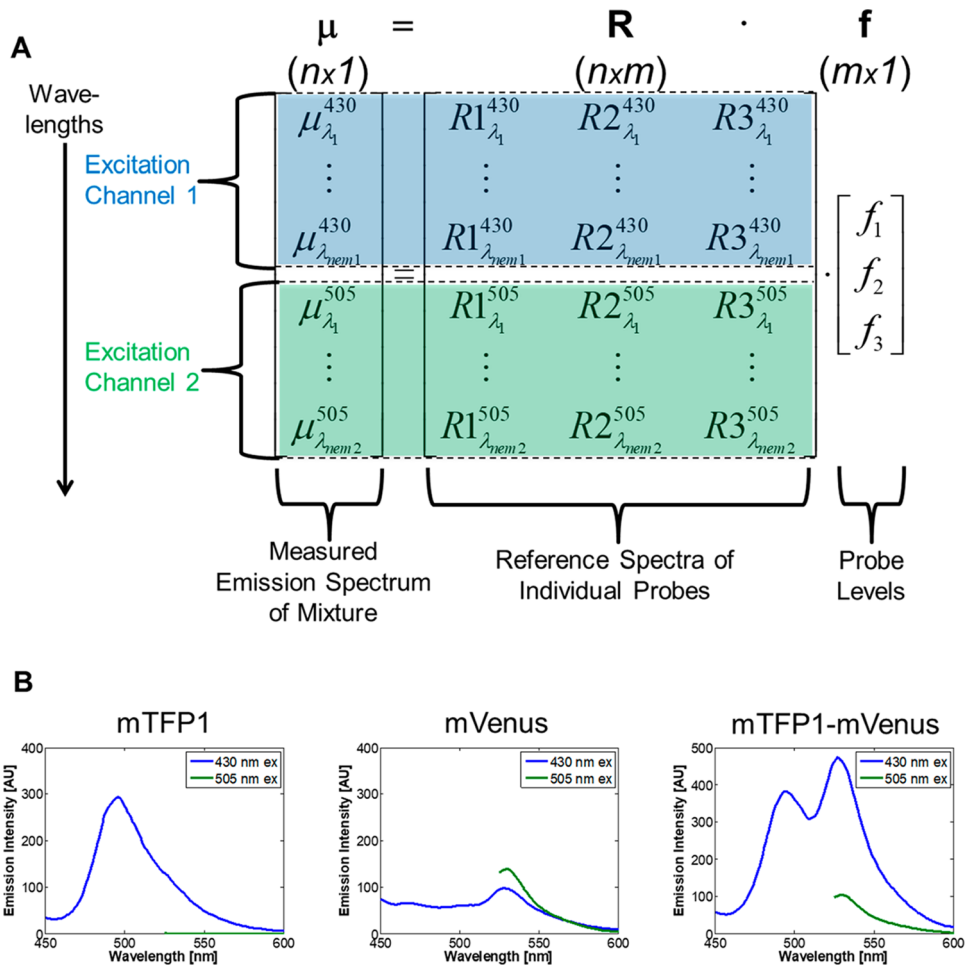

Figure 1. Theoretical basis for multiplexing using spectral imaging and combinatorics (MuSIC). (A) Example arrangement of data for a three probe (m = 3) setup in terms of the linear unmixing equation. Emission spectra data (μ) of a mixture are arranged vertically, stacked by emission wavelength and excitation channel (indicated by color and background highlighting). Each column of the reference matrix is the emission spectra of a probe in isolation, arranged in the same way. (B) Example data for a three probe setup involving a teal fluorescent protein (mTFPl), a yellow fluorescent protein (mVenus), and their covalent fusion (mTFPl-mVenus). Two excitation channels are used, 430 and 505 nm, and fluorescence emission spectra are measured.

acquisition of such MuSIC-compatible data sets increasingly attainable.

RESULTS AND DISCUSSION

Theory. Fluorescence emission follows principles of linear superposition.[2] Therefore, the emission spectra of a mixture of fluorophores can be cast as the sum of its component parts with a matrix equation (Figure 1A).

$$\boldsymbol{\mu} = \mathbf{R}\cdot\mathbf{f} \tag{1}$$

Here, $\boldsymbol{\mu}$ is an n-by-1 vector of measured fluorescence emission intensities at n emission wavelength/excitation channel combinations, $\mathbf{R}$ is the n-by-m matrix of reference emission intensity spectra for m individual fluorescent probes aligned in columns (which could include a column for background fluorescence), and $\mathbf{f}$ is an m-by-1 vector containing the relative levels of the m individual probes. The reference spectra correspond to those of each individual probe in isolation. Note that this equation also can account for multiple n_{ex} excitation channels (Figure 1A).

$$n = \sum_{i=1}^{n_{ex}} n_{emi} \tag{2}$$

where i denotes the excitation channel index and n_{emi} is the number of emission wavelengths measured in that excitation channel. In this case, the rows in every column of the reference matrix $\mathbf{R}$ must be arranged in the same order of excitation channels and wavelengths, along with the measurements $\boldsymbol{\mu}$ (Figure 1A).

Solving eq 1 for $\mathbf{f}$ to infer the relative levels of m individual probes is called "linear unmixing."[4,5] Mathematically, solving for $\mathbf{f}$ requires the rank of the matrix $\mathbf{R}$ to be greater than or equal to m. By increasing the rank of $\mathbf{R}$, one increases the number of individual component levels m that can be independently estimated from fluorescence emission spectra measurements. A typical way to increase the rank of $\mathbf{R}$ is to use multiple excitation channels, which is the intuitive basis for traditional multicolor imaging. Yet, increasing the number of excitation channels does not guarantee increasing the rank of $\mathbf{R}$, because redundant information could be added. For example, exciting yellow fluorescent protein (YFP) variants with 505 and 510 nm light would usually not increase the rank of $\mathbf{R}$ because they are excited in a similar manner by both of these excitation wavelengths.

DOI: 10.1021/acscombsci.8b00101
ACS Comb. Sci. XXXX, XXX, XXX−XXX

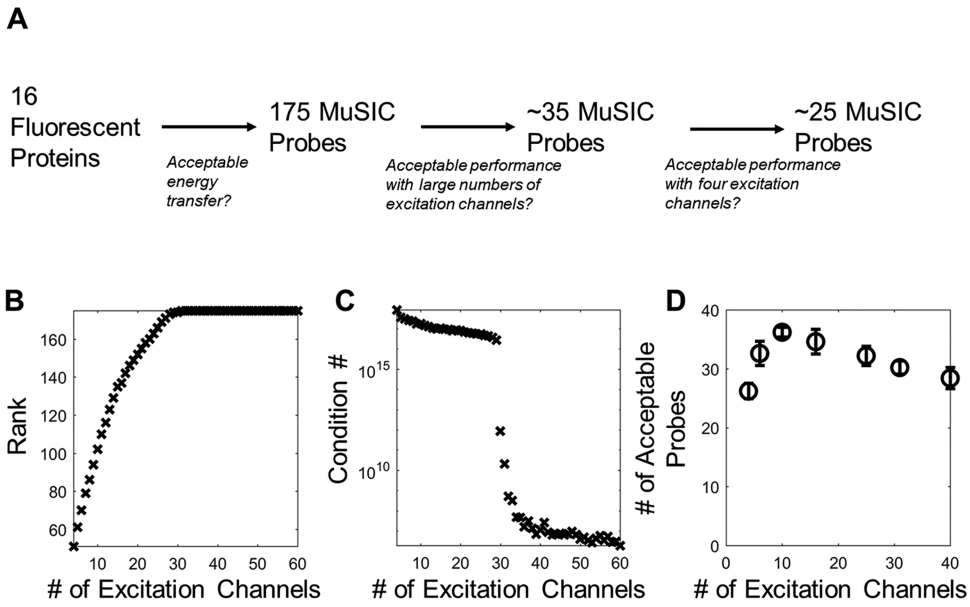

Figure 2. Simulation studies for the potential and limits of MuSIC. (A) Summary of how 16 considered fluorescent proteins are converted into 175 putative MuSIC probes, of which ∼35 have acceptable quantitative behavior using ∼10 excitation channels and ∼25 using four excitation channels. (B) Rankof the reference matrix containing all 175 potential MuSIC probes as a function of the number of excitation channels. Full rank is achieved at 31 excitation channels. (C) Condition number (log scale) of the reference matrix containing all 175 potential MuSIC probes as a function of the number of excitation channels. (D) The number of probes that have a correlation coefficient greater than 0.7 after reducing the number of probes from the original 175, as a function of the number of excitation channels. Error bars denote standard deviation across five probe reduction simulations.

Multiplexing with Spectral Imaging and Combinatorics (MuSIC) works by using covalently linked combinations of fluorophores to add columns to **R** which increase its rank. Each new fluorophore combination has a new column in **R**, and if it increases the rank of **R** by one, then in theory its levels can be estimated through linear unmixing (we use simulation below to explore this more practically with added noise). Consider here a simplistic illustration with experimental data from teal fluorescent protein (mTFP1) and YFP (mVenus; Figure 1B). Although this example will seem trivial, it is intended to convey the essence of the approach in an overtly obvious manner. If one excites at 430 and 505 nm, then mTFP1 and mVenus emission are largely separated by independent excitation, and one can quantify the levels of mTFP1 and mVenus in a mixture, a standard two-color experiment. However, in the spectral emissions from both channels, there is "room to carry" more information, and in particular the red-shifted portion of the 430 nm excitation channel. Because the excitation spectrum of mVenus overlaps with the emission spectrum of mTFP1, they exhibit fluorescence resonance energy transfer (FRET) when in close proximity. By including an mTFP1−mVenus fusion in the experiment, the acceptor mVenus emission becomes strongly visible in the 430 nm channel by FRET (Figure 1B, far right panel). This increases the rank of **R** by one and allows quantification of mTFP1, mVenus, and mTFP1-mVenus levels in a mixture.

This analysis suggests to us that the creation of a new MuSIC fluorescence probe requires that (i) there is sufficient FRET to allow observable fluorescence emission of the acceptor in a new excitation channel and (ii) the resulting emission spectra of the new combination fusion probe is sufficiently distinct from all the other probes in at least one excitation channel. We use these guidelines in the subsequent simulation studies to explore the potential limits of this line of reasoning and more precisely define these sufficiency criteria.

Simulation Studies to Explore Limits and Potential of MuSIC. The above theoretical considerations suggest that MuSIC may offer large increases in fluorescence multiplexing capabilities. However, there are multiple practical questions. How many probes might be multiplexed and their levels estimated simultaneously from a mixture? How many excitation channels might be needed? What spectral emission resolution is sufficient? Are some probe combinations better than others? How robust is the approach to experimental noise? We performed simulation studies to give insight into these questions and guide subsequent experimental efforts (Figure 2A). Specifically, we considered 16 individual fluorescent proteins (FPs): EBFP2,[19] mTagBFP2,[20] mT-Sapphire,[21] mAmetrine,[22] mCerulean3,[23] mTFP1,[24] LSSmOrange,[25] EGFP,[26] TagYFP,[27] mPapaya1,[28] mOrange2,[29] mRuby2,[30] TagRFP-T,[29] mKate2,[31] mCardinal,[32] and iRFP.[33] This is an admittedly small sample, and there are many others available (e.g., refs 34, 35), but this selection was sufficient for a meaningful start. We selected these to span the UV to IR spectrum, for reported photostability, and approximately similar brightness (although this last task is reasonably difficult). We hypothesized that having similar brightness levels would help to increase dynamic range.

The first aspect of this simulation study was to consider how to combine the individual FPs. Bimolecular FRET is common,[36] and trimolecular FRET less so, but has been reported.[37] We therefore exhaustively considered single FPs, dimers, and trimers but filtered all dimers and trimers where FRET efficiency was expected to be <0.2 (based on calculated spectral overlap integral—see Methods). In practice, theoretical FRET can be substantially different from observed FRET. For example, the orientation of the FPs could be suboptimal, or their distance could be further than the Förster radius. However, we reasoned that this consideration of overlap integral was a reasonable starting point for prioritizing certain combinations over others, particularly since this was straightforward to estimate from

DOI: 10.1021/acscombsci.8b00101
ACS Comb. Sci. XXXX, XXX, XXX−XXX

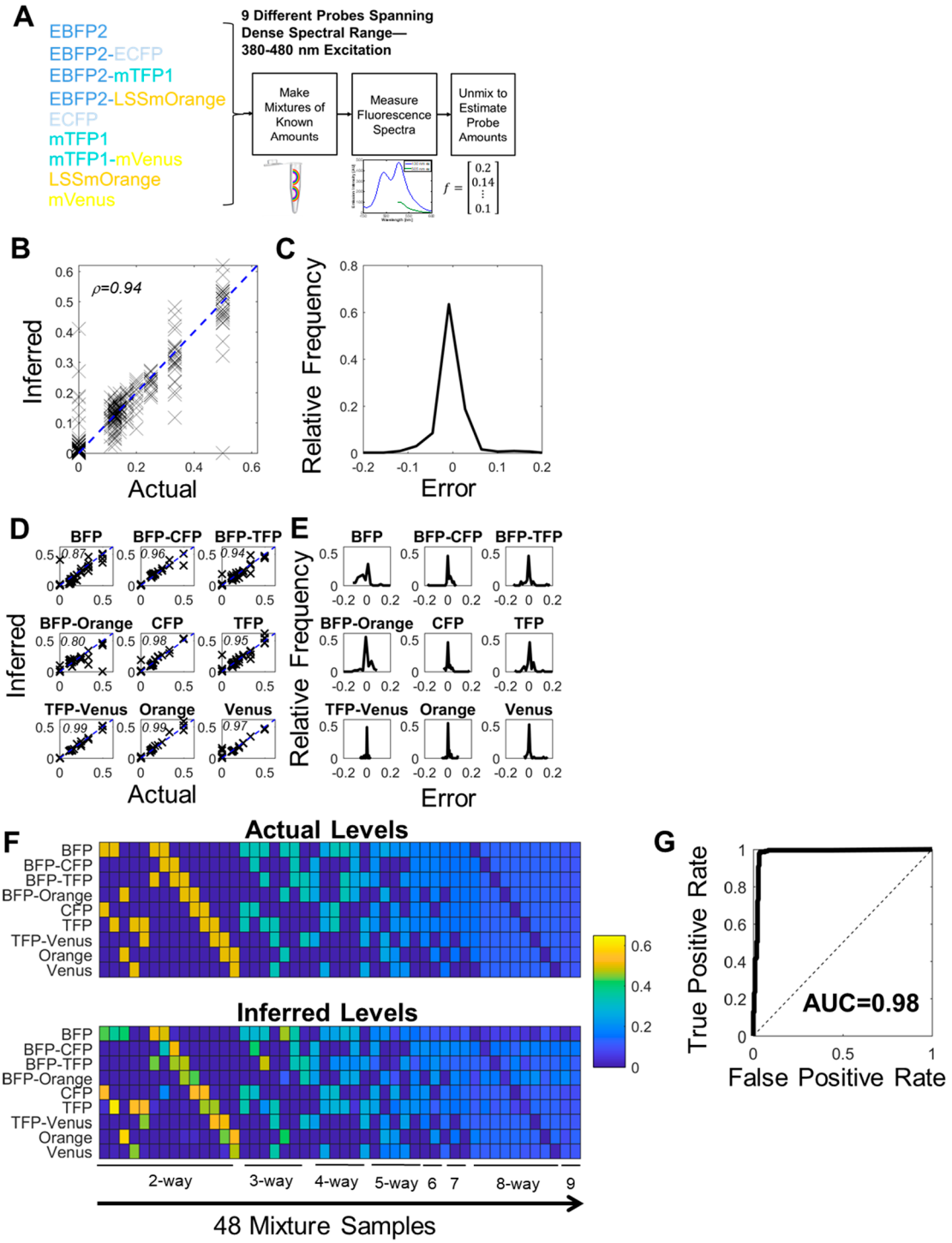

Figure 3. Experimental evaluation of MuSIC. (A) Experimental design. Nine different MuSIC probes were constructed from five fluorescent proteins as indicated. Excitation wavelengths were limited to between 380 and 480 nm. The pure probes were combined into mixtures with known amounts, their emission spectra were measured, and then their levels were estimated via unmixing. These inferred levels were compared to the actual, known levels in the mixture. (B) Aggregate quantitative agreement between actual and inferred levels across mixtures and probes. Dashed blue line is $x = y$; Pearson's correlation coefficient is shown. (C) Histogram of errors, defined as the difference between actual and inferred probe levels, across mixtures and probes. (D,E) Analogous plots as in B and C, respectively, segregated by probe. In D, text in upper left is Pearson's correlation coefficient. (F) Heat maps of quantitative agreement between actual (top) and inferred (below) levels broken down by probe (vertical) and mixture (horizontal). Text below refers to the type of mixture: 2-way means two probes were included in the mixture; 3-way, three; and so on. Color bar indicates relative probe levels. (G) Receiver-operator characteristic (ROC) curve for binary classification of probe presence or absence across the 48 mixtures. The inferred probe level was compared to a threshold for classification as present or absent. This threshold was varied to generate the ROC curve and was uniformly applied across samples and probes. AUC: area under the curve.

available literature data, whereas orientation and distance were difficult to assess without specific experiments. This gave rise to 175 probes that could potentially be quantified from perfect noise free measurements so long as **R** is of full rank (see

DOI: 10.1021/acscombsci.8b00101
ACS Comb. Sci. XXXX, XXX, XXX−XXX

Supporting Information Table S1). However, determining the rank of **R** requires selecting excitation wavelengths.

We first considered a scenario where using a large number of evenly spaced excitation channels between 350 and 700 nm was feasible. We varied the number of excitation channels from four to 60, estimated the relative excitation strength of each probe at each excitation wavelength (from known excitation spectra), and summed the calculated emission intensity in 1 nm increments from 300 to 850 nm (based on the excitation strength, predicted FRET efficiencies, reduced FRET efficiency from direct acceptor excitation, and FP brightnesses—see Methods). There are diminishing returns past 31 excitation channels, where **R** saturates at a full rank of 175 (Figure 2B). The condition number is a metric that can be thought of as quantifying the practical rank of a matrix, where lower numbers indicate a better ability to solve the linear unmixing problem in eq 1. The condition number also starts to decrease sharply around the same number of excitation channels (Figure 2C). However, its magnitude suggests that unmixing performance may be inadequate in terms of % error; values $\sim 10^7$ indicate a likely ill-conditioned matrix, and this large value decreases marginally with increasing number of excitation channels.

We next sought to identify how many probe levels might be reliably quantified using a large number of excitation channels (40), and also how that number of probes changes as the number of excitation channels is reduced down to a more typical four. We simulated multispectral measurements 20 times by sampling probe levels between 0 and 1000 relative concentration units, calculating the expected emission spectra (as above), adding noise to those spectra (similar to what is measured in below experiments), and then unmixing to estimate the probe levels. By adding noise to the simulated data, this allowed us to assess how robust the approach might be in practice. We quantified performance with a Pearson correlation coefficient ρ between the known, randomly sampled levels and estimated, unmixed levels for each of the 175 (or fewer) probes. We progressively eliminated those probes with the lowest correlation coefficient until all probes could be reliably quantified over 3 orders of the sampled concentration magnitude with $\rho > 0.7$ in simulations.

In the case of 40 excitation channels, first we found that the same sets of probes were not recovered in independent simulation runs. This is because adding noise to simulated fluorescence emission spectra data is random, which causes random probes to have the worst correlation coefficient during the removal process. Therefore, we simulated probe removal five independent times for each number of excitation channels considered. We could not pinpoint discernible patterns for which probes were included across multiple simulation runs (full results in Supporting Information Table S2); single, double, and triple probes were prevalent, across the spectrum of available colors. This led us to hypothesize that the number of probes was much more important than probe identity, and that performance would likely have to be assessed experimentally on a probe by probe basis.

For 40 excitation channels, we found roughly 30 probes could be reliably quantified (Figure 2D). Surprisingly, as the number of excitation channels was reduced, this number stayed constant or even slightly increased, all the way to 10 excitation channels where the number of probes was ~35. We speculated that this increase may be due to high quality probes being less likely to be removed during the culling process, although the exact reasons were difficult to pinpoint from the simulation data. With the advent and affordability of white lasers,[38] angle-tuned filters for wavelength scanning,[39,40] large, sensitive multianode photomultiplier tubes,[41] and an ever-increasing number of highly photostable fluorophores, such large excitation channel experiments may become or are already feasible. Below 10 excitation channels, the number of reliable probes decreases, although not drastically. With the current standard of four excitation channels, simulations suggest that approximately 25 MuSIC probes can be reliably quantified in a mixture.

These simulation results suggest that MuSIC may provide a ~6-fold increase over a standard four color experiment, and up to ~8−9 fold if 10 excitation channels are used. They increased our confidence that the approach should be adequately robust to typical levels of experimental noise. Thus, these simulation studies provided important guidelines to aid decision making in the subsequent experimental studies.

Experimental Proof-of-Principal. We wanted to test MuSIC experimentally. Rather than fully expand to the entire spectrum of UV to infrared, we focused on a reduced range of ~25% of the available excitation spectrum from 380 to 480 nm, using the simulation studies above as a guideline for emission spectra every 1 nm, and 10 excitation channels. We reasoned that results here could be expanded and scaled subsequently after determining what caveats and limitations are revealed by reduction to practice that were not uncovered through the theory and simulation studies. This focused us on nine individual or combination probes that we created with fluorescent proteins (FPs; Figure 3A). We cloned, expressed, and purified these proteins (*E. coli*, His tag) and measured the reference spectra of each to verify (i) identity and (ii) appreciable FRET efficiency (Figure S1). Next, we created 48 different mixture samples from these nine individual probes spanning two-way probe combinations to all probes present. We prepared these mixtures in triplicate. We measured the emission spectra of these mixtures in 1 nm increments from 10 equally spaced excitation channels from 380 to 480 nm. From these spectral emission scanning data, we solved eq 1 to estimate the probe levels in each mixture. These "inferred levels" from estimates are compared to the "actual levels" for analysis.

We first evaluated quantitative comparison between actual and inferred levels across all 48 samples and probes in aggregate (Figure 3B,C). This analysis revealed reasonable agreement with most samples falling on or very close to the $x = y$ line (black dashes in Figure 3B; Pearson's $\rho = 0.94$), with only a few outliers away from this curve, and largely unbiased and symmetric error. We parsed these analyses by probe (Figure 3D,E), which revealed that not all probes performed equally. For example, BFP and BFP-Orange were notably more variable than the others ($\rho = 0.87$ and $\rho = 0.80$, respectively), and in ways where the two might be mutually compensating for each other's error when it exists. This may be due to less-than-expected FRET efficiency of the BFP-Orange tandem probe (Figure S1). All the other probes, however, had quite tight error distributions and fell largely along the $x = y$ line ($\rho = 0.94$ to 0.99). These data suggest MuSIC is capable of reasonable quantitative estimation of probe levels from a mixture.

Next, we evaluated agreement between inferred and actual levels by probe and by sample, both quantitatively and with respect to binary classification (Figure 3F,G). Overall, MuSIC does an excellent job of estimating the presence or absence of probes across samples types, from those containing only two probes to those containing most or all probes (Figure 3F). As noted above, the few errors that are noticeable are related to BFP

DOI: 10.1021/acscombsci.8b00101
ACS Comb. Sci. XXXX, XXX, XXX−XXX

and BFP-Orange (e.g., third 2-way sample from the left), which seem to anticorrelate. One way to evaluate the ability of MuSIC to predict whether a probe is present or absent is by constructing a receiver-operator characteristic (ROC) curve (Figure 3G). Here, a cutoff for classifying a probe as present or absent is varied, and the performance of classification based on the actual levels is evaluated in terms of true positive and false positive rate. Random classification falls along the $x = y$ dashed line (AUC = 0.5). MuSIC has excellent classification performance, identifying nearly all true positives before accumulating false positives (area under the ROC curve = 0.98). Thus, we conclude that MuSIC is capable of both quantitative and binary estimation of at least nine probe levels in a mixture using only ∼25% of the available spectrum for excitation. This suggests that future expansion work to the entire spectrum may scale to even greater multiplexing performance. Although we used fluorescent proteins (FPs) here, one can envision mixing and matching both FPs and small molecule fluorophores in a wide potential range of applications, and even bring back in favor fluorophores with complex, multimodal spectra that may have high information content as a MuSIC probe.

■ ASSOCIATED CONTENT

Supporting Information

The Supporting Information is available free of charge on the ACS Publications website at DOI: 10.1021/acscombsci.8b00101.

Supplemental Methods, a detailed description of computational and experimental methods used in this manuscript; Figure S1, normalized emission spectra of individual probes (PDF)

Table S1, probes potentially suited for MuSIC; Table S2, identity of good performing probes after reduction in simulations (XLSX)

MATLAB code to reproduce Figures 2 and 3; entry points to the programs are the files "Fig2.m" and "Fig3.m", which are scripts that generate the figures (ZIP)

■ AUTHOR INFORMATION

Corresponding Author

*E-mail: mbirtwi@clemson.edu.

ORCID

Marc R. Birtwistle: 0000-0002-0341-0705

Author Contributions

M.R.B. conceived of and supervised the work. H.Y.H., M.R.B., A.D.S., M.B., C.M.A., D.P., and S.C. performed the experimental work. M.R.B. performed the simulation work. M.R.B. and H.Y.H. analyzed data. M.R.B. and H.Y.H. wrote the paper.

Notes

The authors declare no competing financial interest.

■ ACKNOWLEDGMENTS

M.R.B. acknowledges funding from Mount Sinai, Clemson University and the NIH Grant R21CA196418. M.B. and A.D.S. were supported by a NIGMS-funded Integrated Pharmacological Sciences Training Program grant (T32GM062754).

■ REFERENCES

(1) Lichtman, J. W.; Conchello, J.-A. Fluorescence microscopy. *Nat. Methods* **2005**, *2*, 910−919.

(2) Zimmermann, T.; Marrison, J.; Hogg, K.; O'Toole, P. Clearing up the signal: spectral imaging and linear unmixing in fluorescence microscopy. *Methods Mol. Biol.* **2014**, *1075*, 129−148.

(3) Goodwin, S.; McPherson, J. D.; McCombie, W. R. Coming of age: ten years of next-generation sequencing technologies. *Nat. Rev. Genet.* **2016**, *17*, 333−351.

(4) Dickinson, M. E.; Bearman, G.; Tille, S.; Lansford, R.; Fraser, S. E. Multi-spectral imaging and linear unmixing add a whole new dimension to laser scanning fluorescence microscopy. *BioTechniques* **2001**, *31*, 1272.

(5) Hiraoka, Y.; Shimi, T.; Haraguchi, T. Multispectral imaging fluorescence microscopy for living cells. *Cell Struct. Funct.* **2002**, *27*, 367−374.

(6) Tsurui, H.; et al. Seven-color fluorescence imaging of tissue samples based on Fourier spectroscopy and singular value decomposition. *J. Histochem. Cytochem.* **2000**, *48*, 653−662.

(7) Carstens, J. L.; et al. Spatial computation of intratumoral T cells correlates with survival of patients with pancreatic cancer. *Nat. Commun.* **2017**, *8*, 15095.

(8) Gorris, M. A. J.; et al. Eight-Color Multiplex Immunohistochemistry for Simultaneous Detection of Multiple Immune Checkpoint Molecules within the Tumor Microenvironment. *J. Immunol.* **2018**, *200*, 347−354.

(9) Coutu, D. L.; Kokkaliaris, K. D.; Kunz, L.; Schroeder, T. Multicolor quantitative confocal imaging cytometry. *Nat. Methods* **2017**, *15*, 39−46.

(10) Pautke, C.; et al. Characterization of eight different tetracyclines: advances in fluorescence bone labeling. *J. Anat.* **2010**, *217*, 76−82.

(11) Padilla-Nash, H. M.; Barenboim-Stapleton, L.; Difilippantonio, M. J.; Ried, T. Spectral karyotyping analysis of human and mouse chromosomes. *Nat. Protoc.* **2007**, *1*, 3129−3142.

(12) Gerdes, M. J.; et al. Highly multiplexed single-cell analysis of formalin-fixed, paraffin-embedded cancer tissue. *Proc. Natl. Acad. Sci. U. S. A.* **2013**, *110*, 11982−11987.

(13) Lin, J.-R.; Fallahi-Sichani, M.; Sorger, P. K. Highly multiplexed imaging of single cells using a high-throughput cyclic immunofluorescence method. *Nat. Commun.* **2015**, *6*, 8390.

(14) Lubeck, E.; Cai, L. Single-cell systems biology by super-resolution imaging and combinatorial labeling. *Nat. Methods* **2012**, *9*, 743−748.

(15) Breen, E. J.; Tan, W.; Khan, A. The Statistical Value of Raw Fluorescence Signal in Luminex xMAP Based Multiplex Immunoassays. *Sci. Rep.* **2016**, *6*, 26996.

(16) Valm, A. M.; et al. Systems-level analysis of microbial community organization through combinatorial labeling and spectral imaging. *Proc. Natl. Acad. Sci. U. S. A.* **2011**, *108*, 4152−4157.

(17) Giesen, C.; et al. Highly multiplexed imaging of tumor tissues with subcellular resolution by mass cytometry. *Nat. Methods* **2014**, *11*, 417−422.

(18) Bendall, S. C.; et al. Single-cell mass cytometry of differential immune and drug responses across a human hematopoietic continuum. *Science* **2011**, *332*, 687−696.

(19) Ai, H.; Shaner, N. C.; Cheng, Z.; Tsien, R. Y.; Campbell, R. E. Exploration of new chromophore structures leads to the identification of improved blue fluorescent proteins. *Biochemistry* **2007**, *46*, 5904−5910.

(20) Subach, O. M.; Cranfill, P. J.; Davidson, M. W.; Verkhusha, V. V. An enhanced monomeric blue fluorescent protein with the high chemical stability of the chromophore. *PLoS One* **2011**, *6*, e28674.

(21) Zapata-Hommer, O.; Griesbeck, O. Efficiently folding and circularly permuted variants of the Sapphire mutant of GFP. *BMC Biotechnol.* **2003**, *3*, 5.

(22) Ai, H.; Hazelwood, K. L.; Davidson, M. W.; Campbell, R. E. Fluorescent protein FRET pairs for ratiometric imaging of dual biosensors. *Nat. Methods* **2008**, *5*, 401−403.

(23) Markwardt, M. L.; et al. An improved cerulean fluorescent protein with enhanced brightness and reduced reversible photoswitching. *PLoS One* **2011**, *6*, e17896.

(24) Ai, H.; Henderson, J. N.; Remington, S. J.; Campbell, R. E. Directed evolution of a monomeric, bright and photostable version of Clavularia cyan fluorescent protein: structural characterization and applications in fluorescence imaging. *Biochem. J.* **2006**, *400*, 531−540.
(25) Shcherbakova, D. M.; Hink, M. A.; Joosen, L.; Gadella, T. W. J.; Verkhusha, V. V. An orange fluorescent protein with a large Stokes shift for single-excitation multicolor FCCS and FRET imaging. *J. Am. Chem. Soc.* **2012**, *134*, 7913−7923.
(26) Cormack, B. P.; Valdivia, R. H.; Falkow, S. FACS-optimized mutants of the green fluorescent protein (GFP). *Gene* **1996**, *173*, 33−38.
(27) Xia, N.-S.; et al. Bioluminescence of Aequorea macrodactyla, a common jellyfish species in the East China Sea. *Mar. Biotechnol.* **2002**, *4*, 155−162.
(28) Hoi, H.; et al. An engineered monomeric Zoanthus sp. yellow fluorescent protein. *Chem. Biol.* **2013**, *20*, 1296−1304.
(29) Shaner, N. C.; et al. Improving the photostability of bright monomeric orange and red fluorescent proteins. *Nat. Methods* **2008**, *5*, 545−551.
(30) Lam, A. J.; et al. Improving FRET dynamic range with bright green and red fluorescent proteins. *Nat. Methods* **2012**, *9*, 1005−1012.
(31) Shcherbo, D.; et al. Far-red fluorescent tags for protein imaging in living tissues. *Biochem. J.* **2009**, *418*, 567−574.
(32) Chu, J.; et al. Non-invasive intravital imaging of cellular differentiation with a bright red-excitable fluorescent protein. *Nat. Methods* **2014**, *11*, 572−578.
(33) Shcherbakova, D. M.; Verkhusha, V. V. Near-infrared fluorescent proteins for multicolor in vivo imaging. *Nat. Methods* **2013**, *10*, 751−754.
(34) Taniguchi, M.; et al. Accessing the near-infrared spectral region with stable, synthetic, wavelength-tunable bacteriochlorins. *New J. Chem.* **2008**, *32*, 947.
(35) McNamara, G.; Gupta, A.; Reynaert, J.; Coates, T. D.; Boswell, C. Spectral imaging microscopy web sites and data. *Cytometry, Part A* **2006**, *69*, 863−871.
(36) Tsien, R. Y.; Bacskai, B. J.; Adams, S. R. FRET for studying intracellular signalling. *Trends Cell Biol.* **1993**, *3*, 242−245.
(37) Pauker, M. H.; Hassan, N.; Noy, E.; Reicher, B.; Barda-Saad, M. Studying the dynamics of SLP-76, Nck, and Vav1 multimolecular complex formation in live human cells with triple-color FRET. *Sci. Signaling* **2012**, *5*, rs3.
(38) Fan, F.; Turkdogan, S.; Liu, Z.; Shelhammer, D.; Ning, C. Z. A monolithic white laser. *Nat. Nanotechnol.* **2015**, *10*, 796−803.
(39) Yu, K.; Liu, Y.; Yin, J.; Bao, J. A novel angle-tuned thin film filter with low angle sensitivity. *Opt. Laser Technol.* **2015**, *68*, 141−145.
(40) Yu, K.; Liu, Y.; Bao, J.; Huang, D. Design of angle-tuned wedge narrowband thin film filter. *Opt. Laser Technol.* **2014**, *56*, 71−75.
(41) Calvi, M.; et al. Characterization of the Hamamatsu H12700A-03 and R12699−03 multi-anode photomultiplier tubes. *J. Instrum.* **2015**, *10*, P09021−P09021.

DOI: 10.1021/acscombsci.8b00101
ACS Comb. Sci. XXXX, XXX, XXX−XXX